THE JOURNAL OF BIOLOGICAL CHEMISTRY VOL. 284, NO. 35, pp. 23697–23707, August 28, 2009
Printed in the U.S.A.

The Phox Domain of Sorting Nexin 5 Lacks Phosphatidylinositol 3-Phosphate (PtdIns(3)P) Specificity and Preferentially Binds to Phosphatidylinositol 4,5-Bisphosphate (PtdIns(4,5)P_2)*[S]◆

Received for publication, April 15, 2009, and in revised form, June 8, 2009 Published, JBC Papers in Press, June 24, 2009, DOI 10.1074/jbc.M109.008995

Leonardus M. I. Koharudin[‡], William Furey[§¶], Hao Liu[‖], Yong-Jian Liu[**], and Angela M. Gronenborn[‡§1]

From the Departments of [‡]Structural Biology, [§]Pharmacology and Chemical Biology, [‖]Neurology, and [**]Neurobiology, University of Pittsburgh School of Medicine, Pittsburgh, Pennsylvania 15260 and the [¶]Biocrystallography Laboratory, Veterans Affairs Medical Center, Pittsburgh, Pennsylvania 15240

Subcellular retrograde transport of cargo receptors from endosomes to the trans-Golgi network is critically involved in a broad range of physiological and pathological processes and highly regulated by a genetically conserved heteropentameric complex, termed retromer. Among the retromer components identified in mammals, sorting nexin 5 and 1 (SNX5; SNX1) have recently been found to interact, possibly controlling the membrane binding specificity of the complex. To elucidate how the unique sequence features of the SNX5 phox domain (SNX5-PX) influence retrograde transport, we have determined the SNX5-PX structure by NMR and x-ray crystallography at 1.5 Å resolution. Although the core fold of SNX5-PX resembles that of other known PX domains, we found novel structural features exclusive to SNX5-PX. It is most noteworthy that in SNX5-PX, a long helical hairpin is added to the core formed by a new α2′-helix and a much longer α3-helix. This results in a significantly altered overall shape of the protein. In addition, the unique double P*XX*P motif is tightly packed against the rest of the protein, rendering this part of the structure compact, occluding parts of the putative phosphatidylinositol (PtdIns) binding pocket. The PtdIns binding and specificity of SNX5-PX was evaluated by NMR titrations with eight different PtdIns and revealed that SNX5-PX preferentially and specifically binds to phosphatidylinositol 4,5-bisphosphate (PtdIns(4,5)P_2). The distinct structural and PtdIns binding characteristics of SNX5-PX impart specific properties on SNX5, influencing retromer-mediated regulation of retrograde trafficking of transmembrane cargo receptors.

The early work on retromer revealed its role in the trafficking of cargo proteins between endosomes and the trans-Golgi network (TGN),[2] although recently, retromer involvement in many other physiological and developmental processes has been uncovered (1, 2). The best studied proteins associated with retromer activity are intracellular sorting receptors such as the yeast vacuolar protein-10 (Vps10) and mammalian mannose 6-phosphate receptors (3, 4). These receptors sort acid hydrolases, enzymes essential for protein degradation, out of the TGN into the yeast vacuole or the mammalian lysosome. Upon releasing their substrates, these cargos traffic back to the TGN to mediate further rounds of cargo-hydrolase transportation. Similar retrograde trafficking of cargo proteins involving signaling molecules such as Wnt and amyloid precursor protein (APP) are thought to be critical for their secretion and function (5, 6). Retrograde transportation is highly regulated by the heteropentameric retromer complex that consists of a sorting nexin (SNX) dimer (*e.g.* Vps5 and Vps17 in yeast) and a Vps26/29/35 trimer (7). In mammals, the binding of the SNX dimer to specific phosphatidylinositol (PtdIns) determines its subcellular membrane association and governs the recruitment of the Vps trimer to endosomal compartments. Mammalian orthologs of the trimer have been biochemically characterized, and their interaction and function in cargo protein trafficking is well established (8). More recently, crystal structures of three Vps proteins in the trimer suggested how this trimer interacts with the SNX dimer and cargo proteins as well as with curved membranes (9–12). In the SNX dimer, SNX1 and SNX2 are thought to be interchangeable Vps5 orthologs (13, 14). The NMR structure of SNX1 revealed details of PI(3)P specific binding, thereby explaining its role in endosomal trafficking (15). The identity for SNX5 as a potential functional mammalian ortholog of Vps17, however, was not revealed until recently.

Although initially identified as a Fanconi anemia complementation group A (FANCA)-binding protein (16), SNX5 was later shown to play an important role in membrane trafficking (17–19). SNX5 contains a PX domain (SNX5-PX) that is the

* This work was supported, in whole or in part, by National Institutes of Health Grants MH62092 and NS058463 (to Y. L.). This work was also supported by startup funds from the University of Pittsburgh School of Medicine (to A. M. G.).

◆ This article was selected as a Paper of the Week.

The atomic coordinates and structure factors (codes 3HPB and 3HPC) have been deposited in the Protein Data Bank, Research Collaboratory for Structural Bioinformatics, Rutgers University, New Brunswick, NJ (http://www.rcsb.org/).

[S] The on-line version of this article (available at http://www.jbc.org) contains supplemental Table S1 and supplemental Figs. S1–S3.

[1] To whom correspondence should be addressed: Dept. of Structural Biology, University of Pittsburgh School of Medicine, 3501 Fifth Ave., BST3/Rm. 1050, Pittsburgh, PA 15260. Tel.: 412-648-9959; Fax: 412-648-9008; E-mail: amg100@pitt.edu.

[2] The abbreviations used are: TGN, trans-Golgi network; SNX, sorting nexin; PX, phox domain; PtdIns, phosphatidylinositol; PtdIns(0)P, phosphatidylinositol phosphate; PtdIns(3)P, phosphatidylinositol 3-phosphate; PtdIns(4)P, phosphatidylinositol 4-phosphate; PtdIns(5)P, phosphatidylinositol 5-phosphate; PtdIns(4,5)P_2, phosphatidylinositol 4,5-bisphosphate; PtdIns(3,4)-P_2, phosphatidylinositol 3,4-bisphosphate; PtdIns(3,5)P_2, phosphatidylinositol 3,5-bisphosphate; PtdIns(3,4,5)P_3, phosphatidylinositol 3,4,5-trisphosphate; MAD, multiwavelength anomalous dispersion; NOE, nuclear Overhauser effect; HSQC, heteronuclear single quantum correlation.

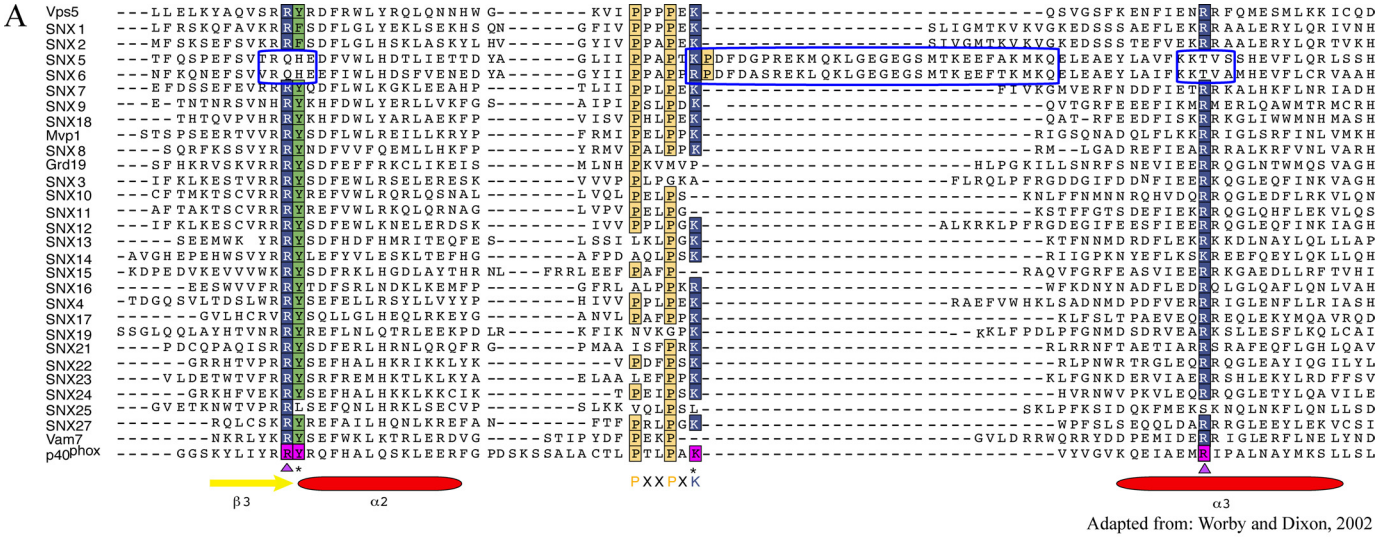

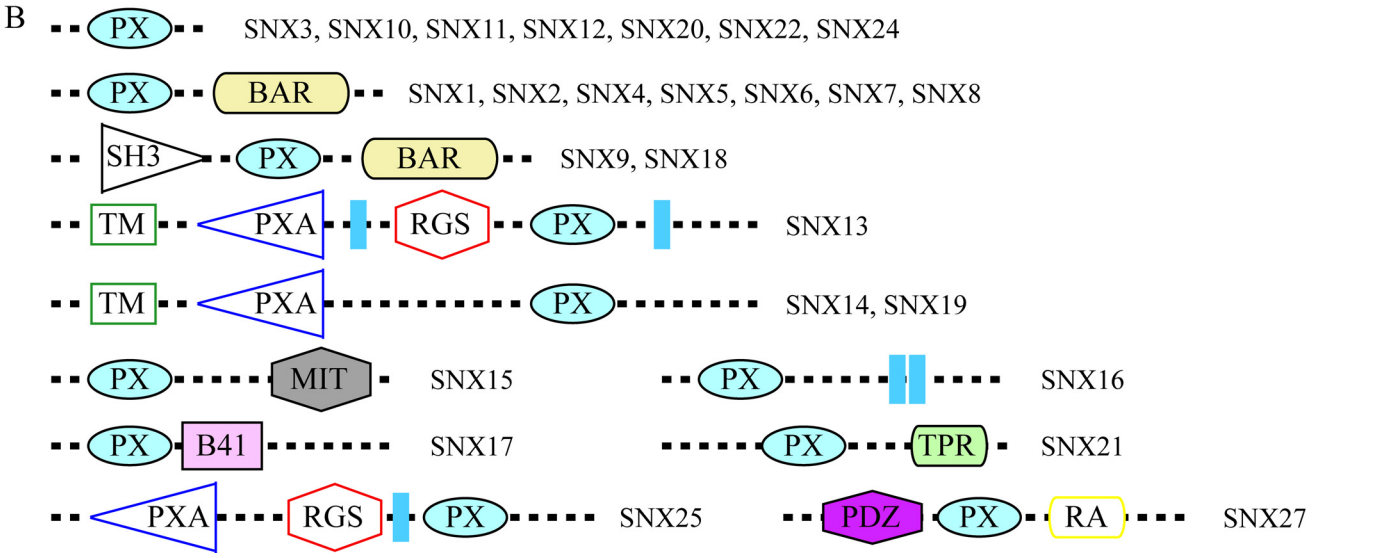

FIGURE 1. **Amino Acid sequence alignment of phox domains and domain architecture of the mammalian sorting nexin family.** *A*, comparative sequence alignment of PX domains for residues equivalent to Gly[49]–Leu[119] of the p40-PX domain (adapted from Worby and Dixon (21)). Prolines in the Pro-*X*-*X*-Pro motif are highlighted in *yellow*, and residues involved in phospholipid binding in the p40-PX domain are *boxed in magenta*. Arg[58] and Arg[105] are marked with *magenta triangles*, and Tyr[59] and Lys[92] are marked with *black stars* at the *bottom* of the sequences. The two conserved Arg residues and Lys[92] of p40-PX in other PX domains are highlighted in *dark blue boxes*; those corresponding to Tyr[59] are *boxed in green*. The secondary structure elements of p40-PX are indicated by *yellow arrows* (β-sheets) and *red ovals* (α-helices). The three sequence stretches that are unique in SNX5-PX (or SNX6-PX) are enclosed in a *bright blue box*. *B*, domain architecture of SNX family members. The four classes within the SNX family are designated as PX SNXs, PX-BAR SNXs, SH3-PX-BAR, and PX-other domain SNXs. Each individual domain is depicted in a different color and/or shape. The following domains are depicted: PX (phox), BAR (Bin-Amphiphysin-Rvs), SH3 (Src homology 3), TM (transmembrane), PXA (PX domain-associated), RGS (regulator of G-protein signaling), MIT (microtubule interacting and trafficking), B41 (band 4.1 homology), TPR (tetratricopeptide repeat), PDZ (postsynaptic protein PSD-95/SAP90, the *Drosophila melanogaster* septate junction protein Discs-large, and the tight junction protein ZO-1), and RA (Ras association).

signature feature in defining the SNX family, composed of 30 members at present (20) (Fig. 1*B*). In addition, SNX5 possesses a C-terminal BAR (Bin/Amphiphysin/Rvs) domain that has been reported to interact with a number of other proteins involved in endosomal trafficking (17, 21–27). It functions as a dimerization module that senses and/or induces membrane curvature (28, 29). Our previous biochemical study suggested a specific interaction between SNX5 and SNX1 through which the two SNXs mutually influence each other's effect in endosomal trafficking of epidermal growth factor receptor upon epidermal growth factor stimulation (17). In support of this observation are several recent reports that indicate a critical role of SNX5 and the closely related SNX6, beyond that of SNX1 and SNX2, on retrograde sorting of mannose 6-phosphate receptor (24, 27). Therefore, SNX5 and SNX6 may be functionally interchangeable orthologs of Vps17 in mammalian cells (7, 24). Furthermore, in contrast to some reports (18, 30), SNX5 partially localizes to late endosomes and the TGN, exhibiting very low binding affinity for PtdIns(3)P (17), the substrate for phox domain proteins associating with early endosome association. Therefore, the subcellular localization and function of the SNX dimer in SNX5 function may depend on its unique structure that is different from other known PX domains.

Most PX domains of SNX family proteins preferentially bind PtdIns(3)P (30–34), with few exceptions that interact with other PtdIns (30, 32, 35). There are about a dozen structurally

characterized PX domains from the SNX family or other PX domain-containing proteins currently deposited in the Protein Data Bank (PDB) data base. Their structures all share common core features, a three-stranded β-sheet that is abutted by three α-helices and an irregular strand containing the P*XX*P region. Analyses of the representative p47-PX and SNX3-PX domain structures suggested that PtdIns(3)P binding involves two conserved Arg residues at positions equivalent to Arg^{58} and Arg^{105} in p40-PX (36). Because equivalent Arg residues are found in the PX domains of most SNX family members, it is generally assumed that all SNX proteins interact with the PtdIns(3)P-enriched elements of the early endocytic compartments. The amino acid sequences of the PX domains of both SNX5 and SNX6, however, lack the two conserved Arg residues that are involved in PtdIns(3)P binding as well as comprising a ~30-residue insertion immediately after the P*XX*P motif (Fig. 1*A*). In addition, the P*XX*P motif is extended into a double P*XX*P motif with the sequence P*XX*P*XX*P. These unique sequence features set SNX5/6 apart from the other SNX family members. In the p40-PX domain and yeast SNX3, the two conserved Arg residues, the loop between the P*XX*P motif, and the α3-helix are involved in forming the binding pocket for the phosphate groups of PtdIns(3)P (36, 37). Therefore, changes in length and sequence in this region in SNX5/6-PX are expected to have profound impact on the specific structure and conformation required for PtdIns recognition.

To elucidate how its unique sequence features influence the function of SNX5 in retromer-mediated retrograde membrane trafficking, we structurally investigated the SNX5-PX domain by NMR spectroscopy and x-ray crystallography. Using direct NMR titrations, we established the PtdIns binding specificity of SNX5-PX. The high resolution (1.5 Å) crystal structure of the domain revealed its distinct features when compared with previously known family members. Our results demonstrate that the SNX5-PX domain is indeed unique, both with respect to its structure as well as with respect to ligand binding. These findings have important implications for the function of SNX5 in the subcellular membrane trafficking and retrograde sorting.

EXPERIMENTAL PROCEDURES

SNX5-PX Expression, Purification, and Crystallization—The SNX5-PX domain (residues 1–180) derived from the rat SNX5 gene was expressed in *Escherichia coli* BL21(DE3) (Stratagene) as a N-terminal His-tagged fusion protein using the vector pET-15B (Novagen). After purification on a Ni^{2+} column (GE Healthcare), fractions were dialyzed into 50 mM Tris-HCl, 100 mM NaCl, 5 mM $CaCl_2$, pH 7.5, and the His tag was cleaved off the protein with thrombin at room temperature overnight. In addition to the canonical thrombin site after the His tag, a secondary cleavage site was discovered between residue Arg^{19} and Ser^{20}. Complete cleavage at this site was allowed to occur (confirmed by mass spectrometry; data not shown). The cleaved protein was separated from the His tag and N-terminal peptide on a Superdex-75 gel filtration column in 20 mM Tris·HCl, 100 mM NaCl, 0.02% NaN_3, pH 8.0. Purified protein fractions were collected and concentrated using Centriprep devices (Millipore).

For crystallization, the protein solution in gel filtration buffer was concentrated to 8 mg/ml. The Se-Met derivative and the 2.19 Å crystals were obtained using an optimized initial crystallization condition of 8 μl of protein *versus* 1 μl of reservoir solution (0.2 M $(NH_4)_2SO_4$, 0.1 M sodium cacodylate trihydrate, pH 6.5, 30% polyethylene glycol 8000) at 4 °C by sitting drop vapor diffusion. The 1.47 Å crystal was obtained using an optimized second crystallization condition (0.2 M NH_4CH_3COO, 0.1 M sodium cacodylate trihydrate, pH 6.5, 30% polyethylene glycol 4000).

Diffraction Data Collection and Structure Determination of the SNX5-PX Domain—The x-ray diffraction data for the Se-Met derivative crystals obtained from the first crystallization conditions were collected at the Southeast Regional Collaborative Access Team(SERCAT) facility sector 22-ID beam line of the Advance Photon Source at the Argonne National Laboratory, Chicago, IL. The MAD data at wavelengths corresponding to the edge, peak, and remote point of the anomalous scattering plots for selenium (0.9795, 0.9793, and 0.9718, respectively) were processed using the d*TREK software (38). The crystal belongs to a primitive orthorhombic space group $P2_12_12_1$ with one molecule per asymmetric unit.

The selenium atom sites and MAD phases after solvent flattening were automatically determined using the program BnP (39). Initial model building with additional iterative density improvement was automatically carried out using the RESOLVE program (40). The generated, incomplete initial model was further refined through cycles of rebuilding and refinement using the program Coot (41) and RefMac (42).

The MAD structure refined at 2.56 Å resolution was used as a molecular replacement model to extend the resolution of the data collected on the home source (Rigaku FR-E generator with a Saturn 944 CCD detector and high flux VariMax optics) for the second, similar crystal form to 2.19 Å. This model was refined to working and free *R*-factors of 23.6 and 28.4%, respectively, using the RefMac program (42) in the CCP4 package (43).

For a crystal obtained using the second condition, a diffraction data set was collected on the home source (Rigaku FR-E generator with a Saturn 944 CCD detector and high flux VariMax optics). The data were processed with the d*TREK software (38). The crystal diffracted to 1.47 Å and belonged to a primitive monoclinic space group $P2_1$, with one molecule per asymmetric unit. The 2.19 Å orthorhombic structure was used as a molecular replacement probe for solving the structure in the monoclinic crystal form. The model was refined to working and free *R*-factors of 18.4 and 23.4%, respectively, using the RefMac program (42) in the CCP4 package (43).

The final model has 98.4 and 1.60% of all residues in the favored and allowed regions of the Ramachandran plot, respectively, and contains no residues in the disallowed region as evaluated by PROCHECK (44). The electron density of the final 1.47 Å resolution map clearly reveals two conformations for 10 side chains (Asn^{26}, Ile^{33}, Ser^{40}, Thr^{78}, Asp^{84}, Ile^{90}, Gln^{107}, Glu^{131}, Ser^{141}, and Ser^{142}). Refinement statistics for all models are provided in supplemental Table S1.

The atomic coordinates of SNX5-PX have been deposited in the RCSB Protein Data Bank under accession codes 3HPB and

3HPC for the 2.19 Å orthorhombic and the 1.47 Å monoclinic crystals, respectively. All structure figures were generated with the atomic coordinates of the monoclinic crystal using the program Chimera (45).

NMR Spectroscopy—NMR spectra were recorded at 25 °C on Bruker AVANCE800, AVANCE700, and AVANCE600 spectrometers equipped with 5-mm triple-resonance, three-axis gradient probes or *z* axis gradient cryoprobes. Spectra for backbone resonance assignments were recorded on a $^{13}C/^{15}N$-labeled sample in 20 mM Tris buffer, 100 mM NaCl, 0.02% NaN_3, pH 7.4. The maximum protein concentration attainable was ~0.5 mM due to limited protein solubility. Three-dimensional HNCACB, CBCA(CO)NH, and ^{1}H-^{15}N NOE spectroscopy HSQC (mixing time 120 ms) experiments (46, 47) were used and allowed for ~99% complete backbone atom chemical shift assignments. All spectra were processed with NMRPipe (48) and analyzed using NMRView (49).

Binding of soluble di-C8 PtdIns (Echelon Biosciences) was investigated at 25 °C by NMR titration experiments using ^{15}N-labeled protein in 20 mM Tris buffer, 100 mM NaCl, 0.02% NaN_3, pH 7.4. Increasing amounts of PtdIns from a stock solution in NMR buffer were added to the protein solution, and ^{1}H-^{15}N HSQC spectra were recorded for each addition up to a final molar ratio of PtdIns:protein of 20:1. Titration isotherms were plotted for four resonances that exhibited sizable and saturable shifts and no peak overlap or broadening. Dissociation constants were calculated by non-linear best fitting the data for four ^{1}HN titration curves simultaneously using KaleidaGraph (Synergy Software, Reading, PA).

RESULTS

SNX5-PX Domain Structure—Structural assessment of SNX5-PX was carried out in solution by NMR spectroscopy for rat SNX5-PX, which exhibits ~99% amino acid sequence identity with the human homolog. The protein sequence comprises Met^{1}–Lys^{180}, His-tagged at the N terminus. However, mass spectrometric analysis of the protein after thrombin cleavage and removal of the His tag revealed that an additional cleavage had occurred between residues Arg^{19} and Ser^{20}. The initial NMR analysis prior to cleavage showed that the first 19 residues of SNX5-PX were highly flexible and essentially unstructured. Therefore, susceptibility to proteolysis is not surprising. The final protein after cleavage and purification that was used for structural work by NMR and crystallography contains residues Ser^{20}–Lys^{180}.

The ^{1}H-^{15}N HSQC spectrum of the protein (Fig. 2) exhibits well dispersed and narrow resonances, indicative of a well folded, monomeric structure. Complete backbone assignments were achieved using three-dimensional HNCACB, CBCA(CO)NH, and ^{1}H-^{15}N NOE spectroscopy HSQC spectra. For the C-terminal residues (Leu^{172} to Arg^{175}), two sets of resonances are observed, most likely caused by nonspecific cleavage of the protein at the C terminus. This was confirmed by mass spectrometry.

The x-ray structure of the SNX5-PX domain was determined at 1.47 Å resolution. Clear electron density was observed for residues Val^{21}–Val^{174}. Ser^{20} and the last six C-terminal residues exhibit high *B*-factors and were excluded from the model as they could not be accurately traced. The overall architecture of SNX5-PX comprises a three-stranded antiparallel β-sheet abutted by three α-helices. In addition, a one-turn 3_{10}-helix that connects helices 4 and 3 and a polyproline region that leads into a long, protruding helical hairpin are present (Fig. 3*A*). The three β-strands are formed by residues Leu^{31}–Glu^{41}, Lys^{44}–Thr^{53}, and Glu^{62}–Arg^{67}, respectively, with β-strand 1 containing a β-bulge between residues Asp^{34} and Pro^{36}. The four α-helices comprise residues His^{69}–Glu^{81} (α1), Asp^{100}–Ser^{115} (α2′), Lys^{118}–Leu^{133} (α3′), Ala^{134}–Ser^{152} (α3), and Arg^{160}–Glu^{167} (α4). Helices α2′ and α3′ are novel features in SNX5-PX that are absent in other known PX domain structures. The α2′-helix follows after the polyproline (P*XX*P*XX*P) region that comprises residues Leu^{88} to Phe^{99}. The short 3_{10}-helix is formed by residues Val^{155}–Lys^{158}. The rest of the structure consists of loops and turns connecting the regular secondary structure elements. At the N terminus, residues Val^{21}–Asp^{28} form a long, irregular strand and exhibit random coil ϕ and φ backbone angles. Interestingly, however, good electron density is observed for these residues because they engage in intermolecular interactions and hydrogen bonding with residues located in the β1-strand of the adjacent molecule (Fig. 3*B*).

Comparison of SNX5-PX with Other PX Domain Structures—The first two PX domain structures that were determined were the NMR structure of p47-PX (50) and the x-ray structure of the p40-PX/PtdIns(3)P complex (36). Currently, 14 different PX domain structures from the SNX family or other PX domain-containing proteins are deposited in the PDB data base (51). These structures are all very similar (Fig. 4*A*), although their sequences exhibit only 6–19% identity with p40-PX. All contain a three-stranded β-sheet abutted by three α-helices and the irregular P*XX*P region. The polyproline motif resides between the first two α-helices (α1 and α2), and the loops that connect strands β1 and β2 and the P*XX*P region with the α2-helix are generally long and not well ordered. The short 3_{10}-helix is present only in a few structures.

Although the core of the SNX5-PX domain resembles that of other known PX domains (Fig. 4*A*), several unique features are present (Fig. 4, *B* and *C*). As mentioned above, a long α-helical hairpin protrudes out from the bottom of the generic PX domain fold. This additional structural element is formed by the new α2′-helix and helix α3′, which is an extension of the common α3-helix in our structure (note that α3 in SNX5-PX is equivalent to α2 in the other PX domain structures). In this manner, a very long helix (α3′ + α3) is created, with α2′ and α3′ forming the helical hairpin (Fig. 4*B*). This helical hairpin comprises all the inserted amino acids between the P*XX*P region and the α3-helix (~30) and is absent in all other SNX-PX domains, except SNX6-PX (Fig. 1*A*). We therefore suggest that the long helical hairpin is the unique structural hallmark of the SNX5-PX domain (and most likely SNX6-PX). The helical hairpin is also present in solution as NMR backbone chemical shifts and NOE connectivities clearly indicate that residues Asp^{100} to Leu^{133} reside in a helical conformation.

Another difference between the SNX5-PX domain structure and other PX domains pertains to the P*XX*P region. In SNX5-PX, this stretch of the polypeptide is very well ordered and packed against the core of the domain, whereas in other known

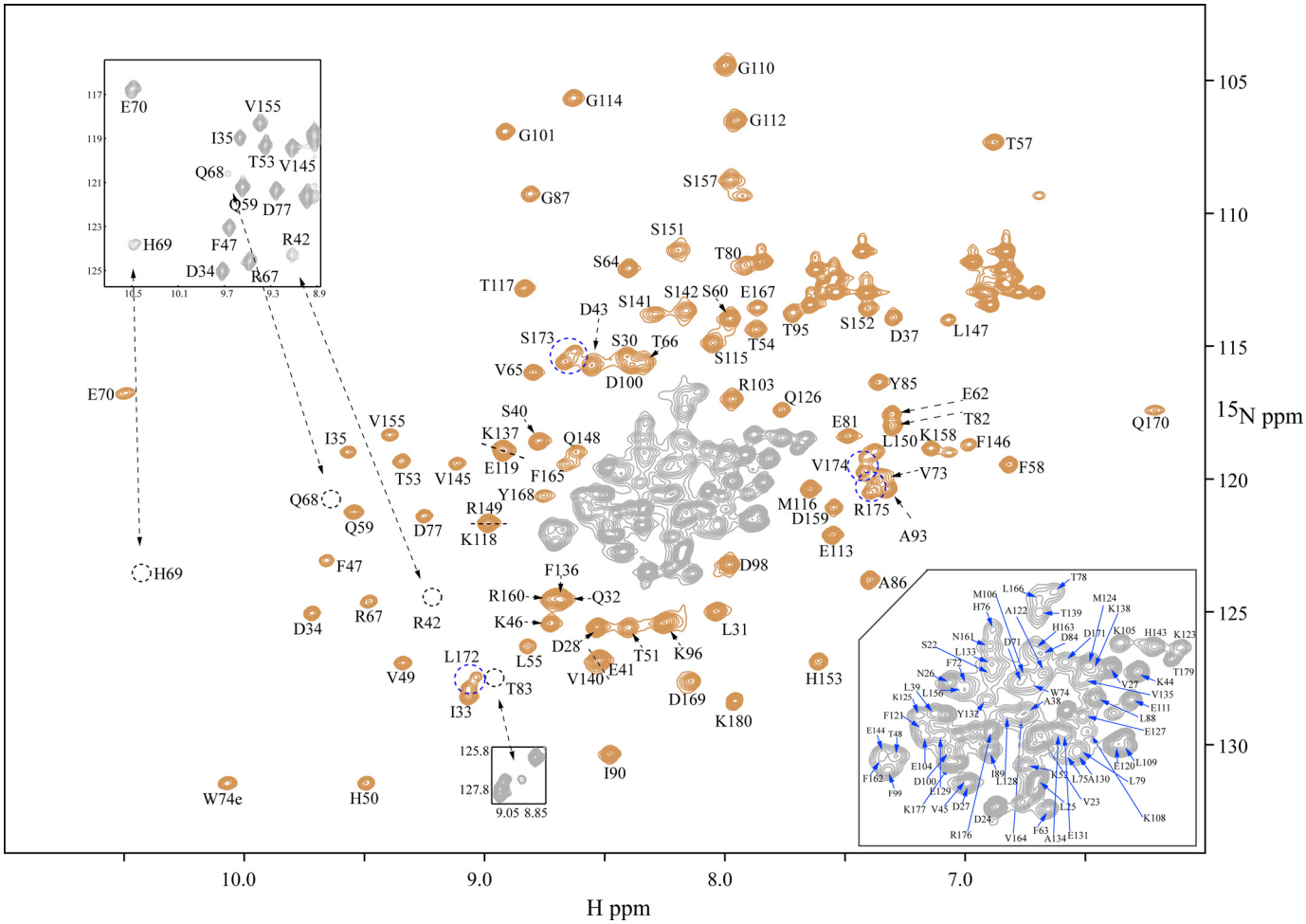

FIGURE 2. **^{1}H-^{15}N two-dimensional HSQC spectrum of SNX5-PX.** Backbone amide resonances are labeled by amino acid type and number. The amides of residues Arg^{42}, Gln^{68}, His^{69}, and His^{83} are marked by *dashed circles*. They exhibit faster solvent exchange than average and therefore are only observed at low contour levels (see *insets*). Assignments for the crowded region in the middle of the spectrum (*gray contours*) are provided in an expansion of this region in the *lower right hand corner* of the spectrum. Note that two sets of resonances are observed for residues Leu^{172}, Ser^{173}, Val^{174}, and Arg^{175} caused by C-terminal heterogeneity (*blue dashed circles*). The spectrum was recorded at 25 °C on a 0.1 mM protein sample in 20 mM Tris buffer, 100 mM NaCl, 0.02% NaN_3, pH 7.4.

PX domain structures, it is irregular and somewhat removed from the rest of the protein (Fig. 4*C*). This is easily appreciated from the comparison of Cα–Cα distances for residues in the polyproline stretch and adjacent ones in the β2-strand. For example, the Cα–Cα distance between Pro^{97} and Val^{45} is ~7.5 Å in the SNX5-PX structure, whereas the equivalent distance between Val^{93} and Phe^{39} in the p40-PX structure is ~13.5 Å. The compactness of this region in SNX5-PX is unlikely the result of crystal packing because this area is solvent-exposed and not involved in crystal contacts with any neighboring molecules (supplemental Fig. S1). The order in this region is most likely caused by the additional P*XX*P motif in the SNX5-PX sequence that is absent in the other SNX sequences (Fig. 1*A*). The extended P*XX*P region comprises the sequence ^{91}**P**PA**P**TK**P**^{97}, and the side chains of Pro^{91}, Pro^{94}, and Pro^{97} (bold letters in sequence) engage in hydrophobic interactions with residues on strand β2 and helices α1 and α3. Pro^{91} interacts with Leu^{79}, Phe^{146}, and Leu^{150}, whereas Pro^{94} interacts with Phe^{72} and Phe^{146}. Further important contacts are made between Pro^{97} and the neighboring Phe^{99} side chain and Val^{45}, Phe^{47}, and Thr^{139} located on strand β2 and helix α3, respectively.

The difference in the local structure of SNX5-PX and other PX domains is illustrated for the example of p40-PX in Fig. 4, *C* and *D*. Comparing SNX5-PX with the PtdIns(3)P-bound form of p40-PX clearly shows that the P*XX*P region in p40-PX is located farther away from the β1-β2 tip than in SNX5-PX. Indeed, the Cα–Cα distance between Phe^{39} and Val^{93} in p40-PX (equivalent to residues Val^{45} and Pro^{97} in SNX5-PX) is almost twice that observed in SNX5-PX. This renders the region of the protein somewhat open and potentially allows for easy access of poly(Pro)-interacting proteins. The same applies to yeast SNX3 (ySNX3), both in its complex with PtdIns(3)P and in its ligand-free form (supplemental Fig. S2). It is worth pointing out that this area forms part of the PtdIns(3)P binding pocket in the p40-PX, ySNX3, and other known SNX-PX domains. Therefore, any conformational difference present in the P*XX*P region of SNX5-PX will influence how and which PtdIns binds to SNX5.

Identification of the PtdIns Specificity of SNX5-PX—At the present time, conflicting data with respect to PtdIns specificity have been reported for SNX5. One group described binding to PtdIns(3)P as well as PtdIns(3,4)P_2 (30), whereas Liu *et al.* (17) did not find any interaction with PtdIns(3)P. This discrepancy

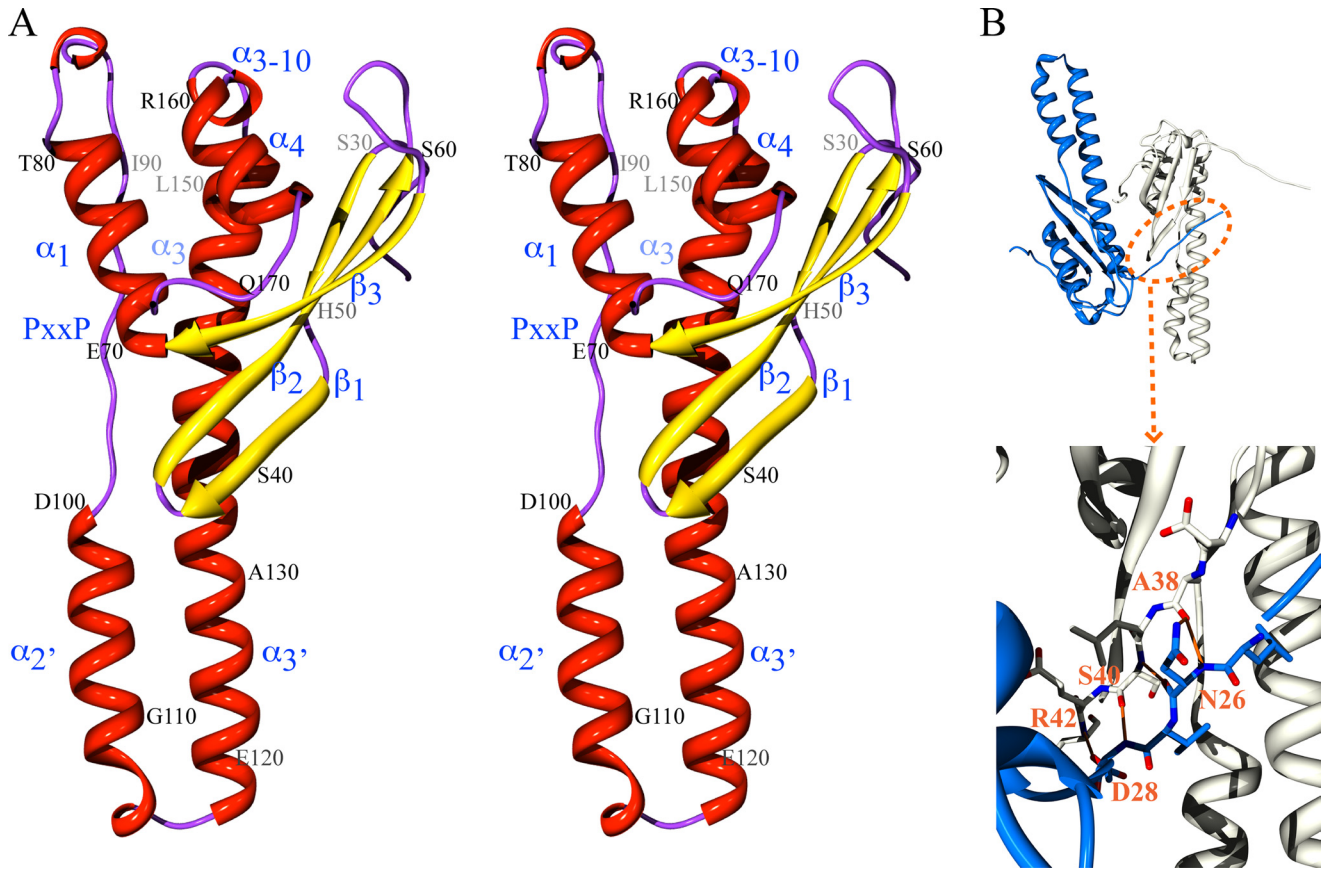

FIGURE 3. **X-ray structure of SNX5-PX domain.** *A*, stereo view of the overall structure of SNX5-PX. β-strands (β1, β2, and β3) and α-helices (α1, α2′, α3′, α3, α_{3-10}, and α4) are colored in *yellow* and *red*, respectively. Residues are numbered at every 10th position. The polyproline (P*XX*P) motif is located in the irregular strand connecting helices α1 and α2′. *B*, intermolecular interaction between the N-terminal residues (Val^{23}–Asp^{28}) of one molecule and the β1-strand of the neighboring one. Backbone hydrogen bonds are formed between the amide of Asn^{26} and the carbonyl oxygen of Ala^{38}, the carbonyl oxygen of Asn^{26} and amide of Ser^{40}, the amide of Asp^{28} and the carbonyl oxygen of Ser^{40}, and the carbonyl oxygen of Asp^{28} and the amide of Arg^{42}.

may be the result of using different protein constructs, different types of assays, and diverse sources of PtdIns. In a liposome binding assay, Merino-Trigo *et al.* (30) used GST-SNX5-PX-(64–166), whereas Liu *et al.* (17) used GST-SNX5-PX-(1–180). Based on our current structure, it is transparent that a protein construct starting at position 64 will not be correctly folded and, in turn, cannot behave like the native, full-length protein. Indeed, our structure clearly shows that the previous domain assignment that positioned the phox domain between residues 64 and 168 based solely on sequence data is incorrect. Experiments using such protein constructs will give erroneous results because the entire three-stranded β-sheet that is important for maintaining the stable architecture of the domain is missing. Therefore, results obtained from binding experiments with SNX5-PX-(64–168) that assign specificity for PtdIns(3)P as well as PtdIns(3,4)P_2 are problematic and should be treated with extreme caution.

With the structure in hand and NMR assignments available, it is possible to directly investigate PtdIns binding to SNX5-PX using NMR titrations. A series of ^{15}N-^{1}H HSQC spectra were recorded for ^{15}N-labeled SNX5-PX (0.1 mM), adding eight different soluble di-C8 PtdIns. In each series, the ligand concentrations were 0, ~0.1, ~0.2, ~0.4, ~0.8, ~1.6, and ~2.0 mM PtdIns. Chemical shift mapping of $^{1}H_N$ and ^{15}N resonances for free and ligand-saturated SNX5-PX allows direct delineation of the ligand binding site on the protein as well as determination of affinities. Consistently, several resonances exhibited small but increasing shifts upon the addition of PtdIns(0)P, PtdIns(3)P, PtdIns(4)P, PtdIns(5)P, PtdIns-(3,4)P_2, PtdIns(3,5)P_2, or PtdIns(3,4,5)P_3 (Fig. 5*A* and supplemental Fig. S3*A*). They include, for example, Arg^{42}, His^{69}, His^{76}, and Arg^{175}. No saturable binding was observed with these seven PtdIns, indicating nonspecific interactions. Mapping of the corresponding residues onto the structure of SNX5-PX also reveals that the affected residues are not confined to a single area in the structure (Fig. 5*E*). In addition, superposition of the two spectra in the presence of ~2.0 mM PtdIns(0)P and PtdIns(3)P (final point of the titrations) were very similar (Fig. 5*B*), indicating that all seven different PtdIns bind in an analogous, very weak, and nonspecific manner to SNX5-PX (see supplemental Fig. S3 for a detailed comparison). In contrast, titration with PtdIns(4,5)P_2 clearly revealed a distinct perturbation profile that mapped to a localized area on the structure (Fig. 5, *C* and *F*). Interestingly, only about half of the non-specifically perturbed residues are affected (Fig. 5, *D* and *F*). Most importantly, the titration with PtdIns(4,5)P_2 exhibited a typical, saturable binding isotherm that is associated with specific binding (Fig. 5*D*, *inset*). Superposition of the ^{15}N-^{1}H HSQC spectra of PtdIns(3)P- and Ptdins(4,5)P_2-bound SNX5-PX (Fig. 5*D*) clearly shows the difference in perturbed resonances (see also

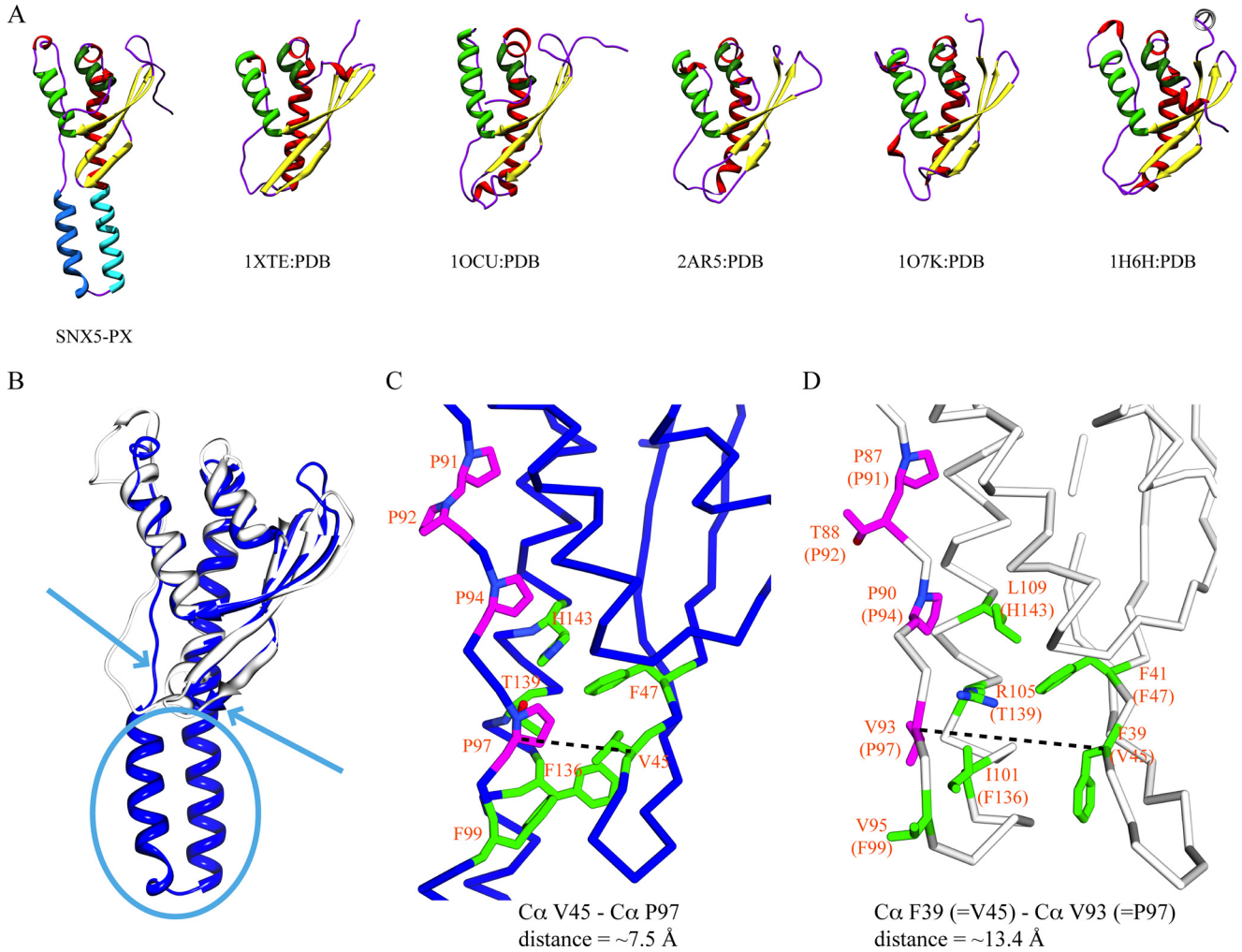

FIGURE 4. **Comparison between the structures of SNX5-PX and selected PX domains.** *A*, architecture of selected structures of PX domains. PX domains used for comparison are as follows: PDB numbers 1XTE (crystal structure of mouse CISK-PX domain), 1OCU (crystal structure of yeast SNX3 (Grd19p), 2AR5 (crystal structure of human C-2 α-phosphatidylinositol 3-kinase), 1O7K (crystal structure of human p47-PX), and 1H6H (crystal structure of human p40-PX). The color coding in the ribbon representations is as follows: all β-strands are shown in *yellow*, helix α1 is in *bright green*, helices α2′ and α3′ in SNX5-PX are in *blue* and *cyan*, and helices α3 and α4 in SNX5-PX and their counterparts (α2 and α3) in other PX domains are in *red* and *dark green*, respectively. *B*, best fit superposition of SNX5-PX (*blue*) and p40-PX (*gray*) structures. The most striking differences are the additional helical insertion at the bottom (*cyan oval*), the altered conformation of the irregular strand that harbors the P*XX*P motif (*cyan arrow*), causing tighter packing of this strand against the body of the protein, and a tighter turn connecting β-strands β1 and β2 (*cyan arrow*). *C*, detailed view of the area around the double P*XX*P motif in SNX5-PX. The compactness is highlighted by indicating the ~7.5 Å Cα–Cα distance between Val[45] and Pro[97]. *D*, detailed view of the corresponding region in p40-PX. In this case, the equivalent Cα–Cα distance between Phe[39] and Val[93] is ~13.5 Å, almost twice that in SNX5-PX.

supplemental Fig. S3 for a detailed comparison). Residues associated with chemical shift changes in the PtdIns(4,5)P_2 titration include Ser[40], Asp[43], Val[45], Lys[44], Lys[46], Asp[98], Phe[99], Asp[100], Arg[103], Lys[105], Glu[113], and Met[116]. The binding constant extracted from the isotherms of four residues (Asp[43], Lys[44], Arg[103], and Lys[105]) yield a K_d value of ~0.41 ± 0.07 mM. Mapping of these specifically perturbed residues onto the structure of the SNX5-PX (Fig. 5*F*) reveals that they are located in two loops, the loop connecting strands β1 and β2 and the loop connecting strands β3 and α1, the P*XX*P region, and the helical hairpin region. Therefore, this region delineates the PtdIns(4,5)P_2 binding site in SNX5-PX. Interestingly, its location is very similar to the PtdIns binding sites that were determined for other PX domains, such as SNX22 (52), Vam7p (34), p40-PX (36), and yeast SNX3 (or Grd19p) (37). We thus conclude that all PX domains bind PtdIns in the same general area, although the specific interactions that position the cognate PtdIns in every individual case are different and unique. Among all eight PtdIns, only PtdIns(4,5)P_2 binds uniquely and specifically to SNX5-PX, establishing unambiguously the ligand specificity of SNX5.

DISCUSSION

Why Does SNX5-PX Lack PtdIns(3)P Specificity?—It is generally accepted that the SNX-PX domain interacts primarily with PtdIns(3)P (30–34), with a few exceptions for which binding to other PtdIns, such as PtdIns(3,4)P_2, PtdIns(3,5)P_2, and PtdIns(3,4,5)P_3, has been reported (30, 32, 35). This binding is mediated by two conserved Arg residues (Arg[58] and Arg[105] in p40-PX (36)), and in the structure of the p40-PX/PtdIns(3)P complex, the guanidinium group of Arg[58] interacts with the 3-phosphate and Arg[105] is hydrogen-bonded to the C-4 hydroxyl of the inositol ring (Fig. 6*A*). In addition to these two critical amino acids, several other residues also contribute to

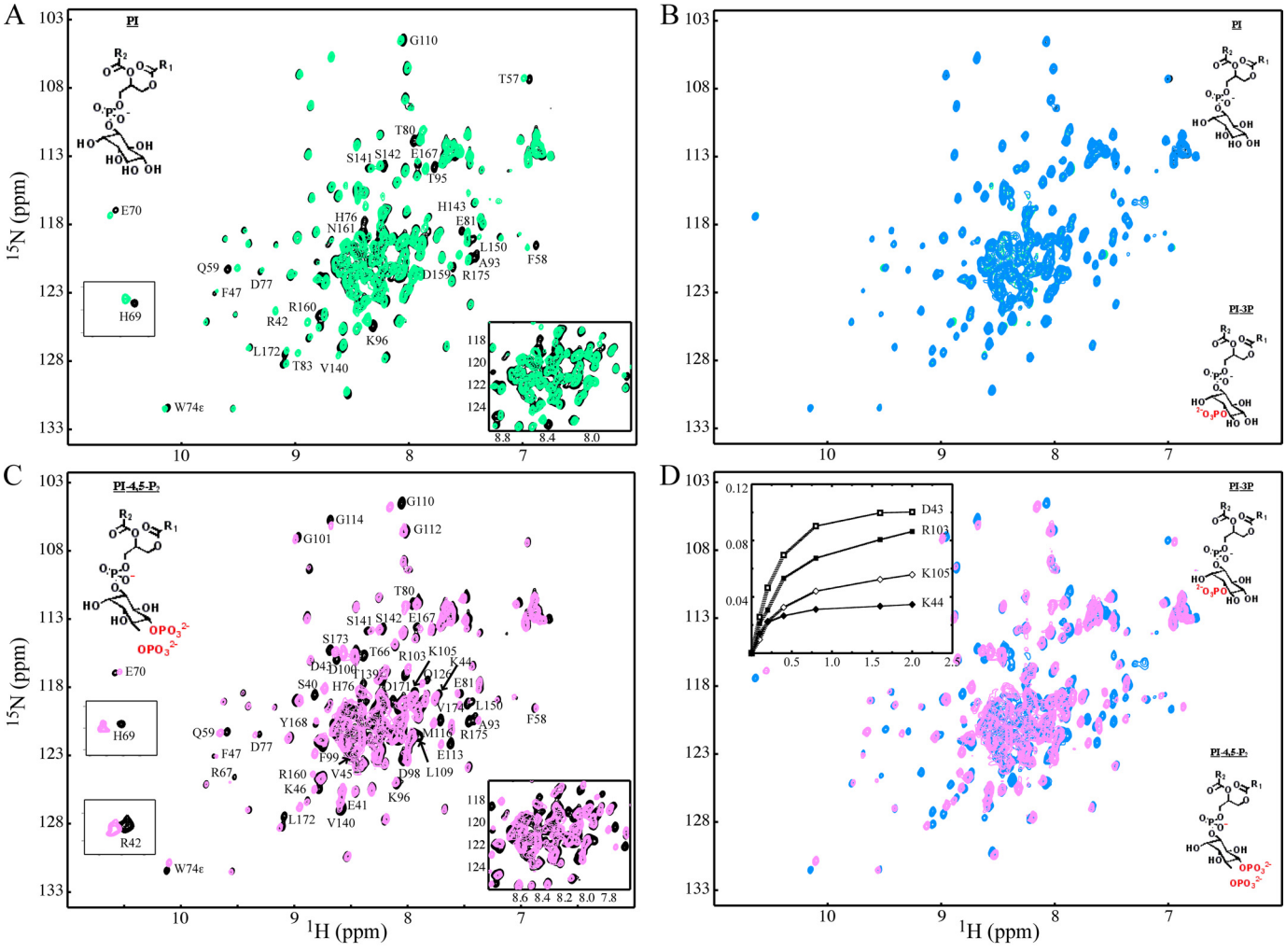
A
PI
B
PI
PI-3P
C
PI-4,5-P2
D
PI-3P
PI-4,5-P2
15N (ppm)
1H (ppm)
H69
R42
E70
W74ε
D43
R103
K105
K44

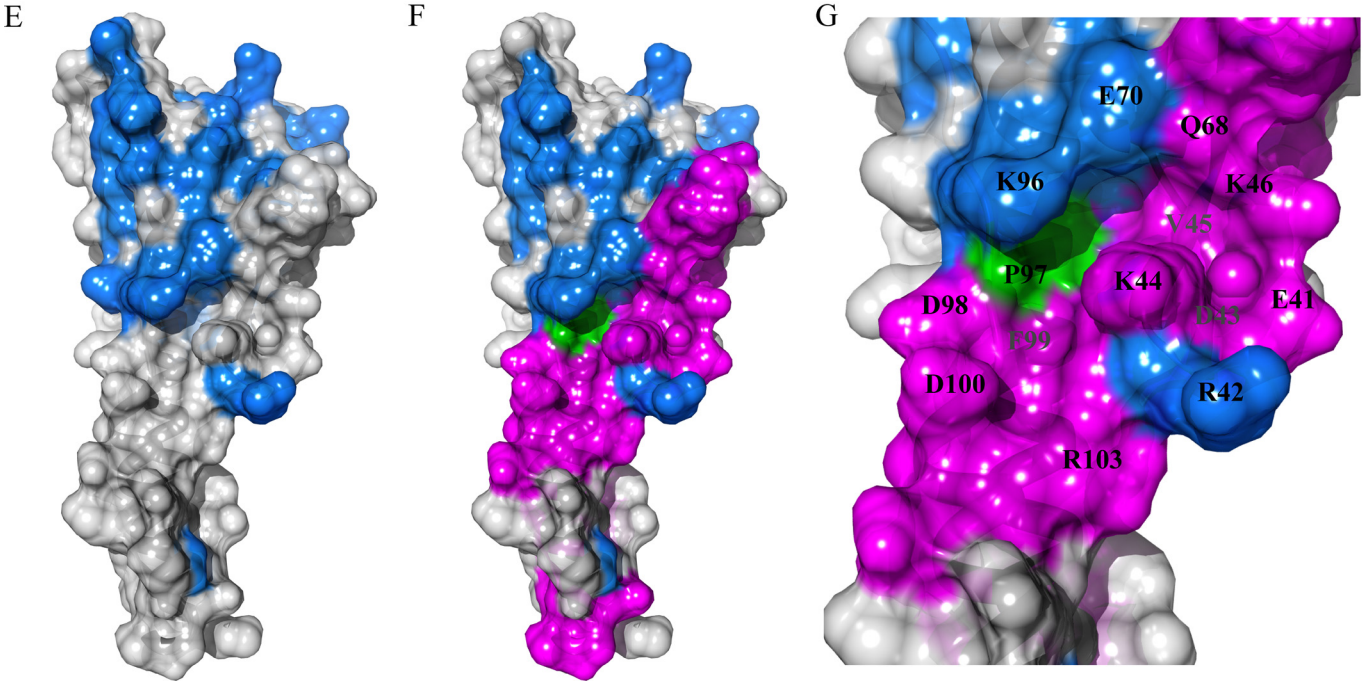
E
F
G
E70
Q68
K96
K46
V45
P97
K44
D98
E41
D43
F99
D100
R42
R103

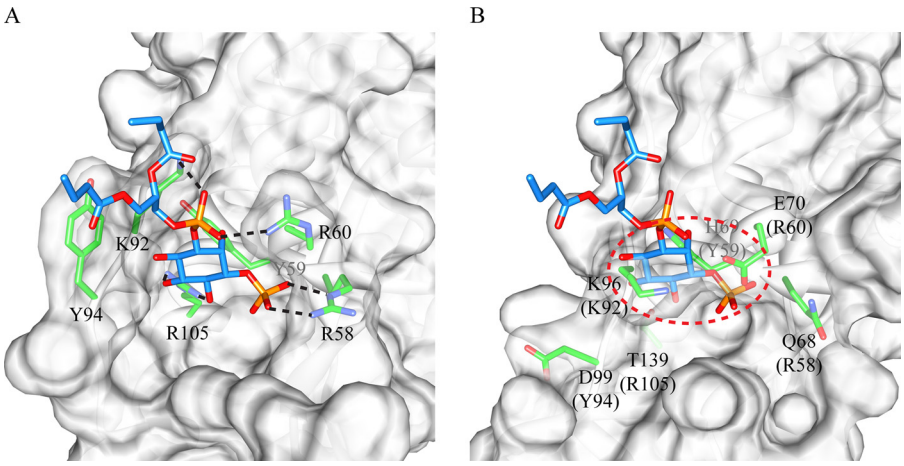

FIGURE 6. **Side-by-side view of the PtdIns binding sites in the p40-PX/PtdIns(3)P complex and in SNX5-PX.** The proteins are show in *space-filling representation*, and the ligand and selected side chains are show in in *ball-and-stick representation*. *A*, contacts between the positively charged Arg[58], Arg[60], Lys[92], and Arg[105] side chains and the negatively charged phosphate or hydroxyl groups on the PtdIns(3)P ligand in the p40-PX/PtdIns(3)P complex structure are shown by *dashed lines*. Tyr[59] and Tyr[94] side chains involved in stabilizing the inositol ring and the acyl chain, respectively, are also *highlighted*. *B*, PtdIns binding site in free SNX5-PX into which a PtdIns(3)P ligand was positioned in the same orientation as in the p40-PX/PtdIns(3)P structure. Note the presence of severe steric clash between Glu[70] and the phosphate group at the C-3 position and between Lys[96] and the inositol ring.

PtdIns(3)P binding. For example, Arg[60] and Arg[92] are engaged in charge-charge interactions with the phosphate group at the C-1 position, Tyr[59] packs against the inositol ring, and Tyr[94] interacts with the acyl chain of the PtdIns(3)P.

In SNX5-PX, the equivalent amino acids are not conserved; most importantly, the two pivotal Arg residues are replaced by Gln[68] and Thr[139], amino acids with clearly very different chemical properties. The replacement of Arg[58] in p40-PX with Gln[68] in SNX5-PX is expected to have a similar effect to the R58Q mutation in p40-PX, which is known to eliminate PtdIns(3)P binding, disrupting localization to the PtdIns(3)P-enriched early endosomes (31). The effect of substituting Arg[105] with Thr[139] in SNX5-PX can be appreciated by comparing the respective regions in the SNX5 and p40 phox structures (Fig. 6). In particular, the conformation of the P*XX*P region is dramatically changed. In the p40-PX/PtdIns(3)P complex structure, the Arg[105] side chain protrudes out of the cleft formed by the P*XX*P strand and β2 (Figs. 4*C* and 6*A*), with the P*XX*P region positioned away from strand β2. Indeed, the presence of the positively charged Arg side chain may help to open up this region, providing access to the ligand. In contrast, in the SNX5-PX structure, the short side chain of Thr[139] is buried and cannot reach the hydroxyl group of the inositol (Fig. 6*B*). Furthermore, positioning the PtdIns(3)P ligand in the same orientation as seen in p40-PX results in severe steric clashes between the Arg[60] and Lys[92] side chains and PtdIns(3)P, rendering such interaction highly unfavorable. Therefore, both the lack of the two specifically interacting Arg residues as well as the overall structural change in this region are most likely responsible for the inability of SNX5-PX to bind PtdIns(3)P.

Based on the results of direct NMR titrations, we concluded that SNX5-PX specifically interacts with PtdIns(4,5)P_2. The question therefore arose how this PX domain accommodates the two phosphate groups attached to the inositol ring of PtdIns(4,5)P_2 and how it distinguishes between PtdIns(4,5)P_2 and the closely related PtdIns(3,4)P_2. Inspection of the structure of PtdIns(3)P in the p40-PX/PtdIns(3)P complex suggests that the C-3 and C-1 phosphate groups will point in the same direction (Fig. 6*A*), whereas a phosphate group at the C-5 position would point in the opposite direction. The PtdIns(4,5)P_2 binding surface determined by NMR chemical shift mapping (Figs. 5*G* and 6*B*) contains a preponderance of positively charged residues including Arg[42], Lys[44], Lys[46], Lys[96], and Arg[103], all of which may contribute to the interaction with the two phosphate groups. This overall feature is reminiscent of the PtdIns binding site on AP180 (53), which is located on the surface of the proteins and recognizes PtdIns(4,5)P_2 through a pool of positive charges. Therefore, the recognition of PtdIns by SNX5-PX is clearly different from that in yeast SNX3 or p40-PX, where the binding pocket lies in a groove formed between the flexible P*XX*P region and the loop connecting strands β1 and β2.

Binding between SNX5-PX and PtdIns(4,5)P_2 is weak, and the low affinity is easily understood from the shallow, surface-exposed ligand binding site. In this context, it should be pointed out that NMR is ideally suited to detect and delineate weak interactions. Although solution NMR experiments were carried out with the water-soluble form of PtdIns, di-C8 PtdIns(4,5)P_2 most likely mimics the individual components of PtdIns(4,5)P_2-containing liposomes. Because PtdIns(4,5)P_2 is the most abundant phosphoinositide, accounting for ~1% of all lipid molecules in the plasma membrane in a typical mammalian cell (at least 25-fold higher than other PtdIns) (54), the weak interactions will be sufficient in localizing SNX5-PX specifically to membrane domains. In addition, the presence of the BAR domain in SNX5, also a membrane interaction domain, will synergistically enhance the overall affinity for PtdIns(4,5)P_2-containing mem-

FIGURE 5. **NMR titration and chemical shift mapping of PtdIns binding to SNX5-PX.** *A*, superposition of the ^{1}H-^{15}N HSQC spectra of free (*black*) and PtdIns(0)P-saturated (*green*) SNX5-PX. *B*, superposition of the ^{1}H-^{15}N HSQC spectra of PtdIns(0)P-saturated (*green*) and PtdIns(3)P-saturated (*blue*) SNX5-PX. *C*, superposition of the ^{1}H-^{15}N HSQC spectra of free (*black*) and PtdIns(4,5)P_2-saturated (*magenta*) SNX5-PX. *D*, superposition of the ^{1}H-^{15}N HSQC spectra of PtdIns(3)P-saturated (*blue*) and PtdIns(4,5)P_2-saturated (*magenta*) SNX5-PX. Titration curves for selected resonances (Asp[43], Lys[44], Arg[103], and Lys[105]) are shown in the *inset*. *E*, structural mapping of residues affected non-specifically by PtdIns(3)P binding. The protein is displayed in *gray surface representation*, and residues whose resonances are perturbed in the titration are colored in *blue*. *F*, structural mapping of residues affected specifically by PtdIns(4,5)P_2. The protein is displayed in *gray surface representation*, and residues whose resonances are perturbed in the titration are colored in *magenta*. *G*, detailed depiction of the PtdIns(4,5)P_2 binding site in SNX5-PX. Selected residues are labeled by residue name and number. Pro[97] is shown in *green*.

branes through the well known avidity effect associated with linking two binding domains.

SNX5 and Retrograde Trafficking—The identification of PtdIns(4,5)P_2 as the specific ligand for SNX5, in combination with its three-dimensional structure, allows us to revisit the role of SNX5 in retromer membrane trafficking. To date, SNX5 involvement in two different pathways has been proposed: (i) SNX5 is a constituent of the retromer complex with activity in regulating transport between endosomes and the TGN (7, 24, 27) and (ii) SNX5 functions as a membrane adaptor and acts in trafficking between the plasma membrane and early/sorting endosomes in the process of micropinocytosis (18, 19, 30). Both scenarios can be reconciled with SNX5-PX interacting with PtdIns(4,5)P_2. In addition to residing in the plasma membrane, PdtIns(4,5)P_2 has also been implicated in TGN sorting (55). Although only low levels of PdtIns(4,5)P_2 were detected in Golgi membranes of mammalian cells and its function is largely unknown, phosphatidylinositol-4-phosphate 5-kinase (PI4P5K) activity at the TGN and several Golgi-associated PdtIns(4,5)P_2 effector proteins, such as phospholipase D (PLD) and dynamin 2, are well documented (56–58). The presence of PtdIns(4,5)P_2 and PtdIns5(P)-phosphatase OCRL1 at the TGN further supports a role of PdtIns(4,5)P_2 in TGN sorting (55). Through forming an SNX dimer with SNX1 via the BAR domains (7, 17, 23, 24, 27), SNX5 may play a role in one of the sequential steps of retromer recycling at the TGN, forming, exiting, and dissociating the retromer complex, with recognition of PtdIns(4,5)P_2 by SNX5-PX constituting the initial step in these dynamic processes. Interestingly, our own data also suggested SNX5 involvement in the maturation of the secretory granule in the regulated secretory pathway of PC12 cells.[3] This suggests a role of SNX5 at the TGN for exporting secretory proteins. On the other hand, if recruited to the plasma membrane where PdtIns(4,5)P_2 is highly enriched, SNX5 may interact with this lipid, with binding further enhanced by its BAR domain as well as recruitment of other membrane-interacting proteins. Observations that SNX5 is transiently associated with the plasma membrane upon epidermal growth factor stimulation and its involvement in the micropinosome support this notion (18, 19, 30). Interestingly, SNX5 is thought to interact with CHC22, the muscle isoform of the clathrin heavy chain, through the coiled-coil domain present in both partners (25), suggesting a potential involvement of SNX5 in membrane invagination in the early stages of clathrin-mediated endocytosis, similar to the role of epsin (59).

Acknowledgments—We thank Dr. Patrick van der Wel for critical reading of the manuscript and Mike Delk for technical support.

REFERENCES

1. Bonifacino, J. S., and Rojas, R. (2006) *Nat. Rev. Mol. Cell Biol.* **7,** 568–579
2. Vergés, M. (2008) *Int. Rev. Cell Mol. Biol.* **271,** 153–198
3. Willnow, T. E., Petersen, C. M., and Nykjaer, A. (2008) *Nat. Rev. Neurosci.* **9,** 899–909
4. Ghosh, P., Dahms, N. M., and Kornfeld, S. (2003) *Nat. Rev. Mol. Cell Biol.* **4,** 202–212
5. Eaton, S. (2008) *Dev. Cell* **14,** 4–6
6. Mayeux, R., and Hyslop, P. S. (2008) *Lancet Neurol.* **7,** 2–3
7. Bonifacino, J. S., and Hurley, J. H. (2008) *Curr. Opin. Cell Biol.* **20,** 427–436
8. Seaman, M. N. (2005) *Trends Cell Biol.* **15,** 68–75
9. Shi, H., Rojas, R., Bonifacino, J. S., and Hurley, J. H. (2006) *Nat. Struct. Mol. Biol.* **13,** 540–548
10. Wang, D., Guo, M., Liang, Z., Fan, J., Zhu, Z., Zang, J., Zhu, Z., Li, X., Teng, M., Niu, L., Dong, Y., and Liu, P. (2005) *J. Biol. Chem.* **280,** 22962–22967
11. Collins, B. M., Skinner, C. F., Watson, P. J., Seaman, M. N., and Owen, D. J. (2005) *Nat. Struct. Mol. Biol.* **12,** 594–602
12. Hierro, A., Rojas, A. L., Rojas, R., Murthy, N., Effantin, G., Kajava, A. V., Steven, A. C., Bonifacino, J. S., and Hurley, J. H. (2007) *Nature* **449,** 1063–1067
13. Carlton, J., Bujny, M., Peter, B. J., Oorschot, V. M., Rutherford, A., Mellor, H., Klumperman, J., McMahon, H. T., and Cullen, P. J. (2004) *Curr. Biol.* **14,** 1791–1800
14. Rojas, R., Kametaka, S., Haft, C. R., and Bonifacino, J. S. (2007) *Mol. Cell. Biol.* **27,** 1112–1124
15. Zhong, Q., Watson, M. J., Lazar, C. S., Hounslow, A. M., Waltho, J. P., and Gill, G. N. (2005) *Mol. Biol. Cell* **16,** 2049–2057
16. Otsuki, T., Kajigaya, S., Ozawa, K., and Liu, J. M. (1999) *Biochem. Biophys. Res. Commun.* **265,** 630–635
17. Liu, H., Liu, Z. Q., Chen, C. X., Magill, S., Jiang, Y., and Liu, Y. J. (2006) *Biochem. Biophys. Res. Commun.* **342,** 537–546
18. Kerr, M. C., Lindsay, M. R., Luetterforst, R., Hamilton, N., Simpson, F., Parton, R. G., Gleeson, P. A., and Teasdale, R. D. (2006) *J. Cell Sci.* **119,** 3967–3980
19. Lim, J. P., Wang, J. T., Kerr, M. C., Teasdale, R. D., and Gleeson, P. A. (2008) *BMC Cell Biol.* **9,** 58
20. Xu, Y., Seet, L. F., Hanson, B., and Hong, W. (2001) *Biochem. J.* **360,** 513–530
21. Worby, C. A., and Dixon, J. E. (2002) *Nat. Rev. Mol. Cell Biol.* **3,** 919–931
22. Carlton, J., Bujny, M., Rutherford, A., and Cullen, P. (2005) *Traffic* **6,** 75–82
23. Teasdale, R. D., Loci, D., Houghton, F., Karlsson, L., and Gleeson, P. A. (2001) *Biochem. J.* **358,** 7–16
24. Wassmer, T., Attar, N., Bujny, M. V., Oakley, J., Traer, C. J., and Cullen, P. J. (2007) *J. Cell Sci.* **120,** 45–54
25. Towler, M. C., Gleeson, P. A., Hoshino, S., Rahkila, P., Manalo, V., Ohkoshi, N., Ordahl, C., Parton, R. G., and Brodsky, F. M. (2004) *Mol. Biol. Cell* **15,** 3181–3195
26. Yoo, K. W., Kim, E. H., Jung, S. H., Rhee, M., Koo, B. K., Yoon, K. J., Kong, Y. Y., and Kim, C. H. (2006) *FEBS Lett.* **580,** 4409–4416
27. Hara, S., Kiyokawa, E., Iemura, S., Natsume, T., Wassmer, T., Cullen, P. J., Hiai, H., and Matsuda, M. (2008) *Mol. Biol. Cell* **19,** 3823–3835
28. Peter, B. J., Kent, H. M., Mills, I. G., Vallis, Y., Butler, P. J., Evans, P. R., and McMahon, H. T. (2004) *Science* **303,** 495–499
29. Dawson, J. C., Legg, J. A., and Machesky, L. M. (2006) *Trends Cell Biol.* **16,** 493–498
30. Merino-Trigo, A., Kerr, M. C., Houghton, F., Lindberg, A., Mitchell, C., Teasdale, R. D., and Gleeson, P. A. (2004) *J. Cell Sci.* **117,** 6413–6424
31. Kanai, F., Liu, H., Field, S. J., Akbary, H., Matsuo, T., Brown, G. E., Cantley, L. C., and Yaffe, M. B. (2001) *Nat. Cell Biol.* **3,** 675–678
32. Cozier, G. E., Carlton, J., McGregor, A. H., Gleeson, P. A., Teasdale, R. D., Mellor, H., and Cullen, P. J. (2002) *J. Biol. Chem.* **277,** 48730–48736
33. Xu, Y., Hortsman, H., Seet, L., Wong, S. H., and Hong, W. (2001) *Nat. Cell Biol.* **3,** 658–666
34. Cheever, M. L., Sato, T. K., de Beer, T., Kutateladze, T. G., Emr, S. D., and Overduin, M. (2001) *Nat. Cell Biol.* **3,** 613–618
35. Zhong, Q., Lazar, C. S., Tronchère, H., Sato, T., Meerloo, T., Yeo, M., Songyang, Z., Emr, S. D., and Gill, G. N. (2002) *Proc. Natl. Acad. Sci. U.S.A.* **99,** 6767–6772
36. Bravo, J., Karathanassis, D., Pacold, C. M., Pacold, M. E., Ellson, C. D., Anderson, K. E., Butler, P. J., Lavenir, I., Perisic, O., Hawkins, P. T., Stephens, L., and Williams, R. L. (2001) *Mol Cell* **8,** 829–839
37. Zhou, C. Z., de La Sierra-Gallay, I. L., Quevillon-Cheruel, S., Collinet, B., Minard, P., Blondeau, K., Henckes, G., Aufrère, R., Leulliot, N., Graille, M.,

[3] Y.-J. Liu, unpublished results.

Sorel, I., Savarin, P., de la Torre, F., Poupon, A., Janin, J., and van Tilbeurgh, H. (2003) *J. Biol. Chem.* **278,** 50371–50376
38. Pflugrath, J. W. (1999) *Acta Crystallogr D Biol. Crystallogr* **55,** 1718–1725
39. Weeks, C. M., Blessing, R. H., Miller, R., Mungee, R., Potter, S. A., Rappleye, J., Smith, G. D., Xu, H., and Furey, W. (2002) *Zeitschrift für Kristallographie* **217,** 686–693
40. Terwilliger, T. C. (2003) *Methods Enzymol.* **374,** 22–37
41. Emsley, P., and Cowtan, K. (2004) *Acta Crystallogr. D Biol. Crystallogr* **60,** 2126–2132
42. Nishida, N., Sumikawa, H., Sakakura, M., Shimba, N., Takahashi, H., Terasawa, H., Suzuki, E., and Shimada, I. (2003) *Nat. Struct. Biol.* **10,** 53–58
43. Collaborative Computational Project, Number 4 (1994) *Acta Crystallogr D Biol. Crystallogr* **50,** 760–763
44. Laskowski, R. A., Macarthur, M. W., Moss, D. S., and Thornton, J. M. (1993) *J. Appl. Crystallogr.* **26,** 283–291
45. Pettersen, E. F., Goddard, T. D., Huang, C. C., Couch, G. S., Greenblatt, D. M., Meng, E. C., and Ferrin, T. E. (2004) *J. Comput Chem.* **25,** 1605–1612
46. Bax, A., and Grzesiek, S. (1993) *Acc. Chem. Res.* **26,** 131–138
47. Sattler, M., Maurer, M., Schleucher, J., and Griesinger, C. (1995) *J. Biomol. NMR* **5,** 97–102
48. Delaglio, F., Grzesiek, S., Vuister, G. W., Zhu, G., Pfeifer, J., and Bax, A. (1995) *J. Biomol. NMR* **6,** 277–293
49. Johnson, B. A., and Blevins, R. A. (1994) *J. Biomol. NMR* **4,** 603–614
50. Hiroaki, H., Ago, T., Ito, T., Sumimoto, H., and Kohda, D. (2001) *Nat. Struct. Biol.* **8,** 526–530
51. Berman, H. M., Westbrook, J., Feng, Z., Gilliland, G., Bhat, T. N., Weissig, H., Shindyalov, I. N., and Bourne, P. E. (2000) *Nucleic Acids Res.* **28,** 235–242
52. Song, J., Zhao, K. Q., Newman, C. L., Vinarov, D. A., and Markley, J. L. (2007) *Protein Sci.* **16,** 807–814
53. Ford, M. G., Pearse, B. M., Higgins, M. K., Vallis, Y., Owen, D. J., Gibson, A., Hopkins, C. R., Evans, P. R., and McMahon, H. T. (2001) *Science* **291,** 1051–1055
54. Stephens, L. R., Jackson, T. R., and Hawkins, P. T. (1993) *Biochim. Biophys. Acta* **1179,** 27–75
55. Choudhury, R., Diao, A., Zhang, F., Eisenberg, E., Saint-Pol, A., Williams, C., Konstantakopoulos, A., Lucocq, J., Johannes, L., Rabouille, C., Greene, L. E., and Lowe, M. (2005) *Mol. Biol. Cell* **16,** 3467–3479
56. Jones, D. H., Morris, J. B., Morgan, C. P., Kondo, H., Irvine, R. F., and Cockcroft, S. (2000) *J. Biol. Chem.* **275,** 13962–13966
57. Godi, A., Pertile, P., Meyers, R., Marra, P., Di Tullio, G., Iurisci, C., Luini, A., Corda, D., and De Matteis, M. A. (1999) *Nat. Cell Biol.* **1,** 280–287
58. Jones, S. M., Howell, K. E., Henley, J. R., Cao, H., and McNiven, M. A. (1998) *Science* **279,** 573–577
59. Ford, M. G., Mills, I. G., Peter, B. J., Vallis, Y., Praefcke, G. J., Evans, P. R., and McMahon, H. T. (2002) *Nature* **419,** 361–366